XI International Conference on Computational Plasticity. Fundamentals and Applications
COMPLAS XI
E. Oñate, D.R.J. Owen, D. Peric and B. Suárez (Eds)

MOLECULAR DYNAMICS SIMULATIONS ON INTERACTION BETWEEN DISLOCATION AND Y_2O_3 NANOCLUSTER IN FE

KISARAGI YASHIRO*, TAKANORI MUTSUKADO†, MINORU TANAKA†, AKIHIRO YAMAGUCHI †, KENJI KOGA ‡, TAKASHI SEGI ‡ AND TAKANARI OKUDA ‡

*Graduate School of Engineering, Kobe University
1-1, Rokkodai, Nada, Kobe, 657-8501, Japan
e-mail: yashiro@mech.kobe-u.ac.jp, http://mm4.scitec.kobe-u.ac.jp/~yashiro/

†Student of Graduate School of Engineering, Kobe University

‡Kobelco Research Institute, Inc.
1-5-5, Takatsukadai, Nishi-ku, Kobe, Hyogo 651-2271, Japan

Key words: Yttria Oxide, ODS Steels, Dislocation, Nano Precipitates, Molecular Dynamics Simulation

Abstract. For a new insight on the mechanical properties of oxide dispersion strengthened (ODS) steels from atomistic viewpoints, we have implemented molecular dynamics simulations on the interaction between Y_2O_3 nanocluster and dislocation in bcc Fe. There is so far no all-round interatomic potential function that can represent all the bonding state, i.e. metal, ion and covalent systems, so that we have adopted rough approximation. That is, each atom in Y_2O_3 is not discriminated but treated as "monatomic" pseudo-atom; and its motion is represented with the simple pairwise potential function as same as Johnson potential for Fe. The potential parameters are fitted to the energy change in the hcp infinite crystal, by using the ab-initio density functional theory (DFT) calculation for explicitly discriminated Y and O. We have set edge/screw dislocation in the centre of periodic slab cell, and approached it to the "YO" monatomic nano-cluster coherently precipitated in bcc-Fe matrix. The dislocation behavior is discussed by changing the size and periodic distance of the nano-cluster. Among the many useful results, we have obtained a conclusion that the edge dislocation is strongly trapped by YO sphere larger than the diameter of $d = 0.9\,\mathrm{nm}$, while the screw dislocation shows various behavior, *e.g.* it cuts through the precipiate without remarkable resistance if the dislocation line tension is high, or it changes the slip plane leaving jogs at the position anterior to the precipiate with loose line tension.

1 INTRODUCTION

Oxide dispersion strengthened (ODS) steels are potential next-gen materials for fuel cladding tubes at nuclear power plants. For the engineering application and further developments of desired steels, it is urgent to understand the key mechaism of their superior properties against neutron irradiation and high temperature. Starting from the pioneering report for alloying elements and mechanical alloying process of ODS steels in 1989 [1], experimental studies have revealed the relationship between internal microstructure and mechanical properties [2], improvement of tensile and creep properties by extremely fine Y-Ti-O clusters with Ti addition [3], quantitative evaluation of nanosized oxides [4], and so on. So far the fine oxides, of a few nanometer size, are expected to prevent the free dislocation motion; however, due to the complexity of mechanical alloying and recrystalization process, it is still difficult to show the direct evidence even with the recent advancement of experimental technique such as TEM *in situ* test.

Computational approach would be one answer to tackle these difficulties. In the field of physics of crystal plasticity, various dislocation-obstacle problems have long been discussed using molecular dynamics (MD) and discrete dislocation dynamics (DDD) simulations; and we have also discussed the dislocation motion in γ/γ' microstructure in Ni-based superalloys [5, 6]. However, there is no suitable potential function which can represent all the bonding state, i.e. metal, ion and covalent systems with sufficient number of atoms needed for deformation simulation. Of course the ab-initio density functional theory (DFT) calculation can treat mixing of any atom species, however, the calculation is so far limited to very small system at most a few hundred atoms. Thus quite a few atomistic simulations can be found for ODS steels except for lattice Monte Carlo (LMC) simulation, in which atom position is restricted on regular lattice site, so that the limited combination of local bonding can be precisely determined by ab-initio DFT calculation. Alinger et al. [7] performed the LMC simulation of Fe-Y-Ti-O system and discussed the structure and morphology of precipitated nanocluster. Hin et al. [8] simulated more realistic precipitation by kinetic LMC, considering the different diffusion mechanism (O atoms by interstitial jumps and Fe and Y atoms by vacancy jumps). Both studies apply finer lattice mesh than the usual bcc lattices and their results should be appreciated as accurate prediction based on DFT data. However, we would confront to drastic increase in the combination of local bonding if we applied these DFT-LMC analysis to many alloy elements system for real ODS steel design. Moreover, we never apply these DFT-LMC scheme to disordered structure, such as dislocations and grain boundaries, since we should consider enormous mesh much more than the number of atoms involved. From an engineering point of view, we need an atomistic simulator in which the potential functions have differentiable form for dynamic simulation and they are also easy to fit for new elements interest. The 2-body potential form is the simplest way and there are many resources fitted for various elements; however, obviously we would fail to represent the bonding between oxygen and metallic atoms if we fitted them separately in the 2-body form. Thus, in the present study, we don't

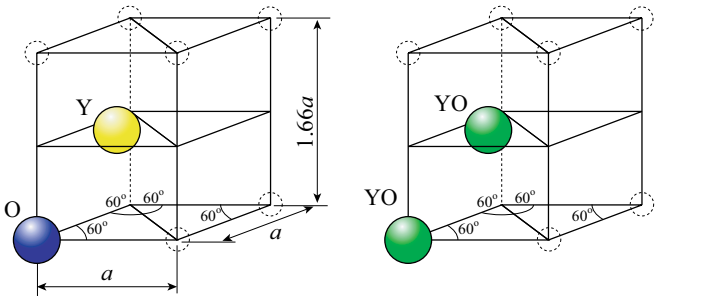

(a) hcp unit cell for DFT calculation (b) hcp unit cell for monatomic "YO"

Figure 1: Rhombohedral unit cells for hcp structure.

distinguish the Y and O atoms in Y_2O_3 but treat as "monatomic" pseudo-atom of YO, in the fitting of Johnson potential parameters against the DFT calculation for explicitly discriminated Y and O. By virtue of this rough approximation, we can easily implement atomistic simulation using conventional resources, *e.g.* Johnson potential parameters for Fe, keeping the rough characteristics of oxides such as lattice parameters and bulk modulus. Although we cannot validate the physical meaning of the isolated pseudo-atom nor discuss the formation and structure of new oxidation products, we can perform MD simulation on the interaction between edge/screw dislocation and oxide nano-cluster. In the present study, we show the brief fitting process and MD simulations of edge/screw dislocation approaching the nano-clusters coherently precipitated in bcc-Fe matrix, changing the size and distances of precipitates.

2 POTENTIAL FITTING PROCEDURE

DFT calculations for potential fitting are implemented using the Vienna Ab-initio Simulation Package (VASP) developed by Kresse and Hafner [9]. Although the Y_2O_3, M_2X_3 type metal oxide, is reported to form the C-rare earth oxide structure [10], it is very difficult to directly consider such a low-symmetric irregular structure by DFT calculation. Thus we have roughly approximated the structure of Y_2O_3 by simple hcp lattice, which is close to the corundum structure or the second candidate of M_2X_3 metal oxide. Figure 1 shows the rhombohedral unit cells for hcp lattice. The supercell for DFT calculation has one Y-atom and one O-atom at the lattice point as shown in Fig. 1(a). Keeping the atom position at the lattice point, or statically, we have changed the lattice parameter a and performed DFT calculation to obtain the energy–lattice parameter curve. The ultrasoft pseudopotential [11] is adopted and the exchange correlation term is treated in the formulation of GGA (generalized gradient approximation) [12]. The cutoff energy and number of **k** points are 296.9 eV and $15 \times 15 \times 15$, respectively.

Johnson potential expresses the system energy, E_{tot}, by the following form:

$$E_{\mathrm{tot}} = \sum_i \sum_{j>i} \left[-C_1 (r_{ij} - C_2)^3 + C_3 r_{ij} - C_4 \right] \tag{1}$$

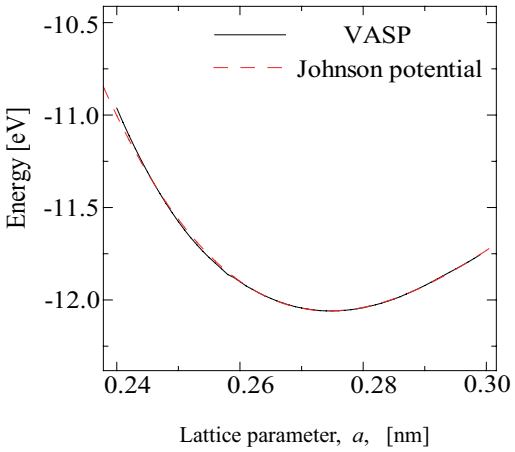

Figure 2: Free-energy curves against lattice expansion/compression by DFT calculation for discriminated Y and O in the hcp structure and by Johnson potential fitted as monatomic YO mean-atom.

Table 1: Potential parameters for Fe and YO pseudo-atom.

Element	Range [nm]	C_1	C_2	C_3	C_4
Fe	$0.19 < r_{ij} < 0.24$	2.1960	3.0979	2.7041	7.4365
	$0.24 < r_{ij} < 0.30$	0.6392	3.1158	0.4779	1.5816
	$0.30 < r_{ij} < 0.344$	1.1150	3.0664	0.4669	1.5480
YO	$0.19 < r_{ij} < 0.344$	0.523	3.090	0.194	1.560

here r_{ij} is the distance between atoms i and j, and the potential parameter $C_1 \sim C_4$ should be found for yttria oxide. We have expressed the infinite YO hcp crystal with monatomic YO pseudo-atoms in Fig. 1(b) under the periodic boundary, and fitted its energy change to the DFT result (Fig. 2). By this fitting process, the equilibrium lattice length and the bulk modulus, or energy change rate against lattice expansion/compression, are precisely represented for monatomic YO pseudo-atoms. On the Fe-YO interaction, simple arithmetic average rule is adopted, i.e., $(C_i^{\mathrm{Fe}}+C_i^{\mathrm{YO}})/2$. All the potential parameters are listed in Table 1.

3 SIMULATION ON EDGE DISLOCATION

3.1 Simulation procedure

Figure 3 shows the dimensions and introduction of edge dislocation. The x, y and z axes are orinented to the [111], [$\bar{1}$12] and [$\bar{1}$10] directions in the bcc structure. For the precipitate–edge dislocation problem, we have replaced Fe atoms with YO ones, in the sphere at the position shown in Fig. 3(a). That is, the precipitate has initially bcc structure or coherently precipitated in the bcc matrix. Different sphere diameter d is

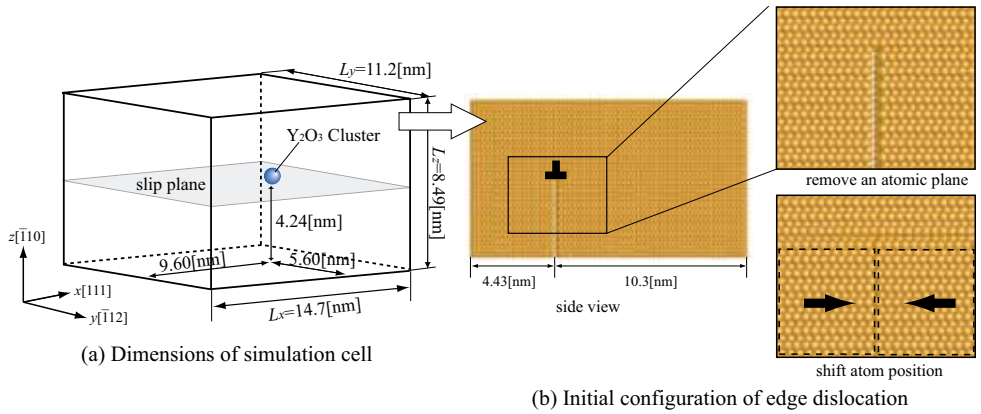

(a) Dimensions of simulation cell

(b) Initial configuration of edge dislocation

Figure 3: Simulation model for edge dislocation.

considered, i.e., 0.6, 0.9, 1.5, 3.0 and 5.0 nm. The edge dislocation is also introduced by eliminating one atomic plane as shown in Fig. 3(b). The periodic boundary condition is applied in the x and y axes, i.e. dislocation motion and line directions, while the z boundary is basically free surface but also has restriction for deformation control. The initial structure is relaxed by MD calculation of 100 000 fs under $T = 10$ K. Then, we apply the small displacement of 1.0×10^{-6} nm at every MD step in the [111] direction for upper z surface atoms and in the opposite for lower ones, in order to approach the edge dislocation to the precipitate. For comparison, we have also performed same shear simulation *without* precipitate. Furthermore, we have also implemented same simulation with different cell length L_y in the y direction to check the effect of the periodic distance between the precipitates. Note that the temperature is so far intentionally controlled to very-low value since we would include not only the mechanical effects but also thermal fluctuation under high temperature, and we couldn't seperate the both effects if we had started from high temperature.

3.2 Results and discussion

Figure 4 summarizes the result of simulations with the cell length of L_y=11.2 nm. Fig. 4(a) shows the position of dislocation core while Fig. 4(b) does the shear stress, τ_{zx}, on the simulation cell. The abscissa is time and the shear simulation starts from $t = 0$ fs. The position of dislocation core is evaluated from the atoms with high energy as marked in Fig. 5(a), one example of dislocation motion. In the figure, only the dislocation and precipitate are visualized with a certain threshold for potential energy. Back to Fig. 4(a), the dislocation begins to glide around $t = 20\,000$ fs and reaches to constant speed before $t = 50\,000$ fs, if there is no precipitate anterior to the dislocation (thick solid line). The shear stress also peaks out and shows constant flow stress at that point of steady motion (Fig. 4(b)). In the case of the YO diameter of $d = 0.6$ nm, the position–time and stress–time curves are very similar to those of without precipitate (dashed lines). That is, the

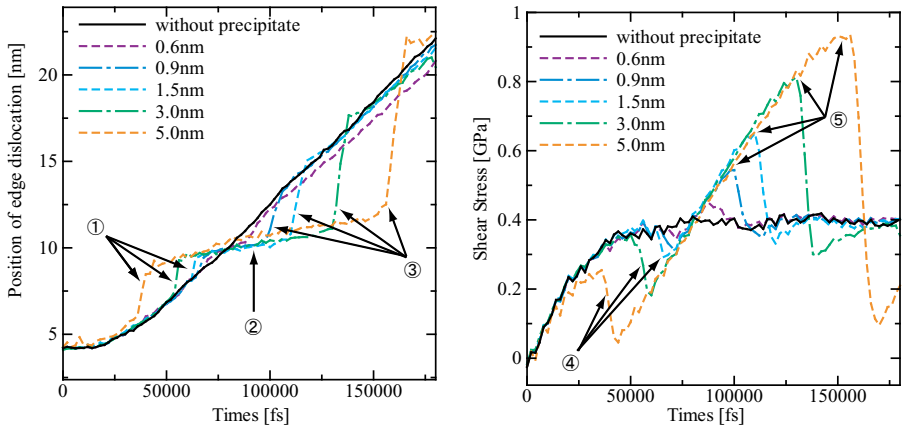

(a) Time–position curves (b) Time–shear stress curves

Figure 4: Change in the core position and shear stress (edge dislocation, $L_y = 11.2\,\mathrm{nm}$).

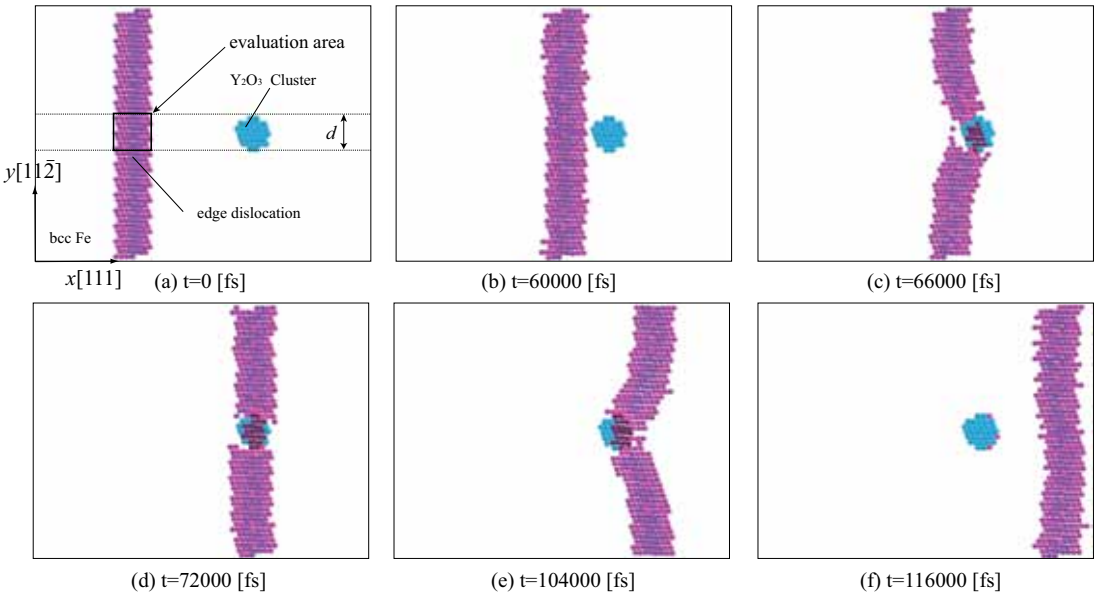

Figure 5: Motion of edge dislocation on the slip plane ($d = 1.5\,\mathrm{nm}$, L_y =11.2 nm).

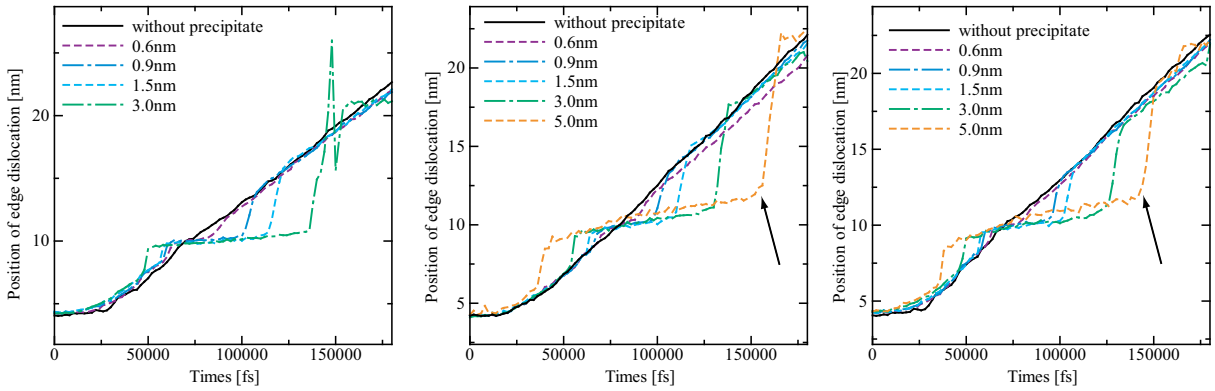

(a) 4.9[nm] (b) 11.2[nm] (c) 25.2[nm]

Figure 6: Position–time curves with different periodic length between precipitates (edge dislocation).

edge dislocation receives no resistance from such small precipitates of $d = 0.6\,\mathrm{nm}$. On the other hand, the dislocation motion is clearly affected by the YO precipitate larger than $d = 0.9\,\mathrm{nm}$, as previously shown in Fig. 5 for $d = 1.5\,\mathrm{nm}$. In the approaching process, the precipitate attracts the edge dislocation as shown in Fig. 5(c). On the other hand, the edge dislocation should largely bend to unlock the pinning (Fig. 5(e)). Both of them are the evidence that the YO precipitate has attractive effect on the edge dislocation. These tendency becomes more remarkable with the precipitate size, as indicated Arrows ① and ③ in Fig. 4(a). It is also noteworthy that the increased shear stress is first relaxed by the collision of dislocation and precipitate as indicated Arrows ④ in Fig. 4(b), while the unlock stress of Arrow ⑤ drastically increases with the precipitate size.

Figure 6 shows the position–time curves with different simulation cells of $L_y = 4.9, 11.2$ and $25.2\,\mathrm{nm}$. Fig. 6(b) is identical to Fig. 4(a). On Fig. 6(a), there is no space between YO precipitates of the diameter $d = 5\,\mathrm{nm}$ in the smallest cell length $L_y = 4.9\,\mathrm{nm}$, so that we omit the simulation. The diameter $d = 3\,\mathrm{nm}$ might be still large for the cell length $L_y = 4.9\,\mathrm{nm}$, since there is large oscillation around $t = 150\,000\,\mathrm{fs}$ where the trapped dislocation is unlocked and proceeds again. With the larger periodic distance or larger spacing between precipitates, the locked dislocation can largely bend. Thus the unlock time becomes shorter as shown with Arrow in Figs. 6(b) and 6(c) with the help of line tension of largely bent dislocation. On the other hand, the smallest precipitate $d = 0.6\,\mathrm{nm}$ is always similar to the case without precipitate, despite of the precipitate spacing.

4 SIMULATION ON SCREW DISLOCATION

4.1 Simulation procedure

Figure 7 shows the simulation model for screw dislocation. The slab cell looks like same as the previous simulation; however, the slip plane is set normal to the $[\bar{1}12]$ direction (y-axis) and periodicity is only set to the [111] direction (x-axis). As mentioned later, the

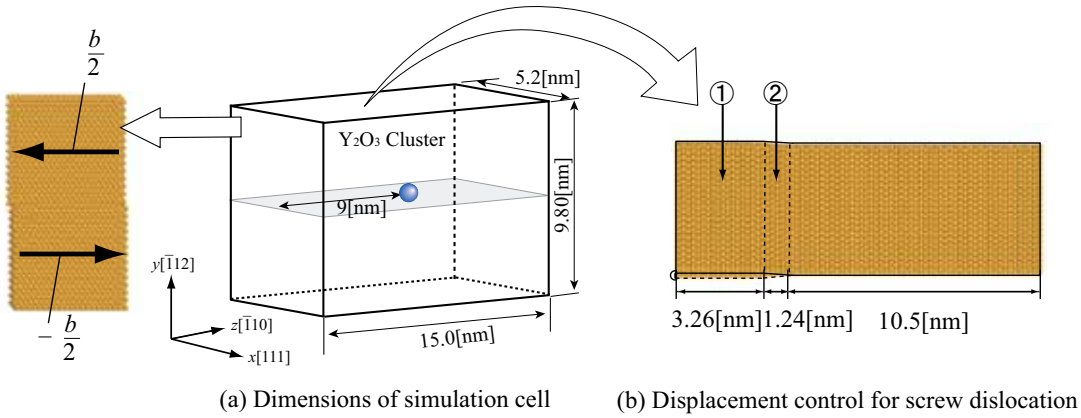

Figure 7: Simulation model for screw dislocation.

screw dislocation tends to change the slip plane so that we adopt narrow periodic length $L_x = 5.2\,\mathrm{nm}$ as the standard length. Atoms in the upper and lower half of $z < 3.26\,\mathrm{nm}$ from the front edge (Area ①) are alternately shifted in the x-axis, with the magnitude of $b/2$ (b; Burgers vector). Atoms in Area ② are also linearly shifted to connect the slipped and non-slipped area. As same as the previous simulations, the initial configuration is relaxed with 100 000 fs MD calculation under $T = 10\,\mathrm{K}$, for both cases with and without YO precipitate. The maximum diameter of the precipitate is $d = 3\,\mathrm{nm}$. Then, small displacement of $3.0 \times 10^{-6}\,\mathrm{nm}$ is applied in the [111] and $[\bar{1}\bar{1}\bar{1}]$ directions alternately on the upper and lower surfaces of the cell, to proceed the screw dislocation by the xy shear.

4.2 Results and discussion

Figure 8 shows the position–time and shear stress-time curves in the cell width of $L_x = 5.2\,\mathrm{nm}$. The horizontal dashed line in Fig. 8(a) indicates the center of YO precipitate. Also, the vertical broken lines in Figs. 8(a) and 8(b) mark the same time points. Contrary to the edge dislocation, there is no remarkable difference even with the large ($d \geq 0.9\,\mathrm{nm}$) precipitate. Figure 9 shows one example of dislocation motion in the simulation of $d = 1.5\,\mathrm{nm}$. Despite of the similar line tension as the previous Fig. 6(a), the screw dislocation feels no resistance to cut through the precipitate, leaving high energy atoms around the YO atoms. On the other hand, if we use the wider simulation cell of $L_x = 10.4\,\mathrm{nm}$, the dislocation shows various motion as indicated in the position of dislocation core in Fig. 10(b). Here Fig. 10(a) is identical to Fig. 8(a). The mechanism for the variation in Fig. 10(b) is different case by case; for example, the screw dislocation changes its slip plane and drags the jog-like high energy atoms at the point far away from the precipitate, and passes the precipitate–matrix interface as shown in Fig. 11 of $d = 0.9\,\mathrm{nm}$. In the case of $d = 3.0\,\mathrm{nm}$, the screw dislocation does change the slip plane too, but is attracted and trapped by the precipitate and leaves Orwan loop like defect around the precipitate

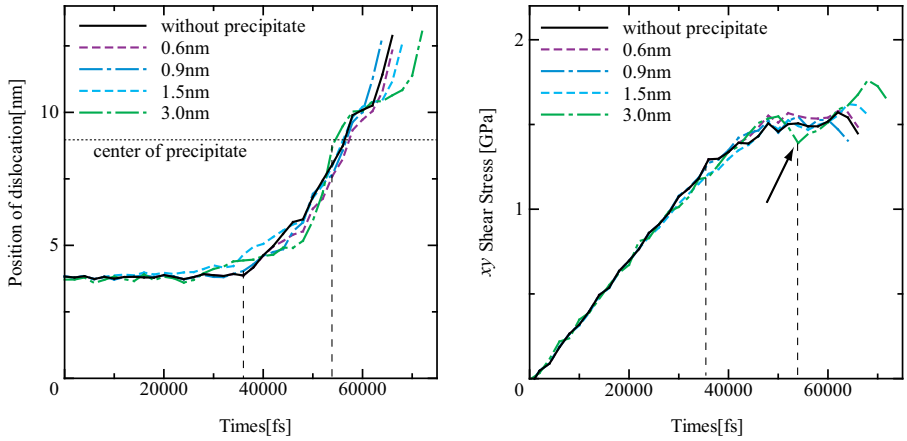

(a) Time–position curves (b) Time–shear stress curves

Figure 8: Change in the core position and shear stress (screw dislocation, $L_x = 5.2\,\mathrm{nm}$).

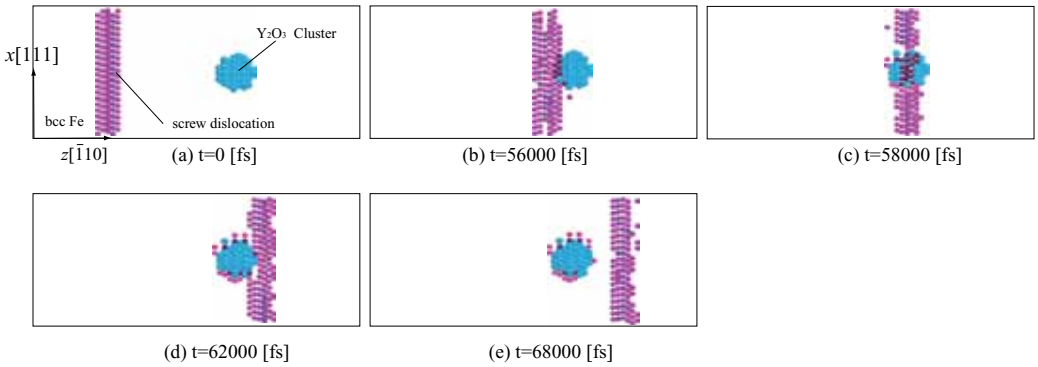

Figure 9: Motion of screw dislocation (L_x=5.2 nm, $d = 1.5\,\mathrm{nm}$).

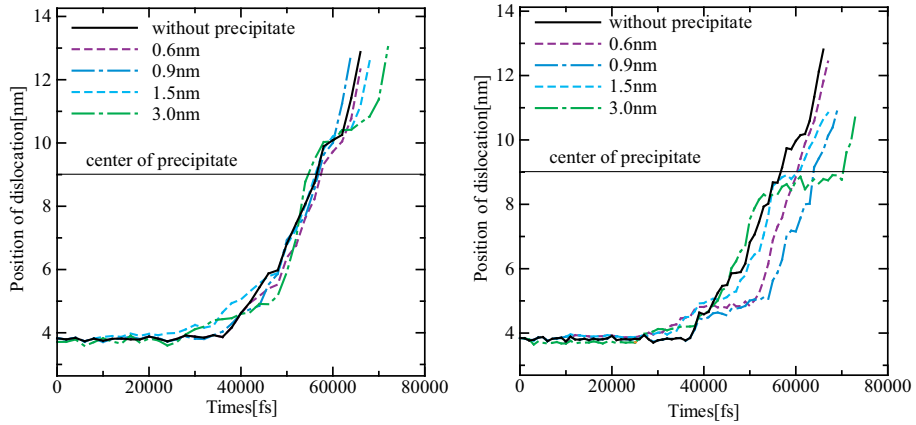

(a) 5.2[nm] (b) 10.4[nm]

Figure 10: Position–time curves with different periodic length between precipitates (screw dislocation).

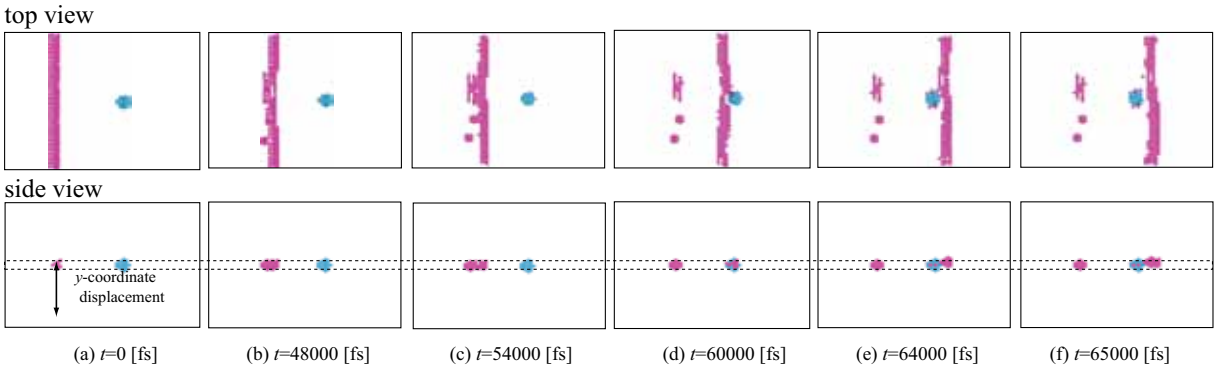

Figure 11: Motion of screw dislocation (L_x=10.4 nm, d = 0.9 nm).

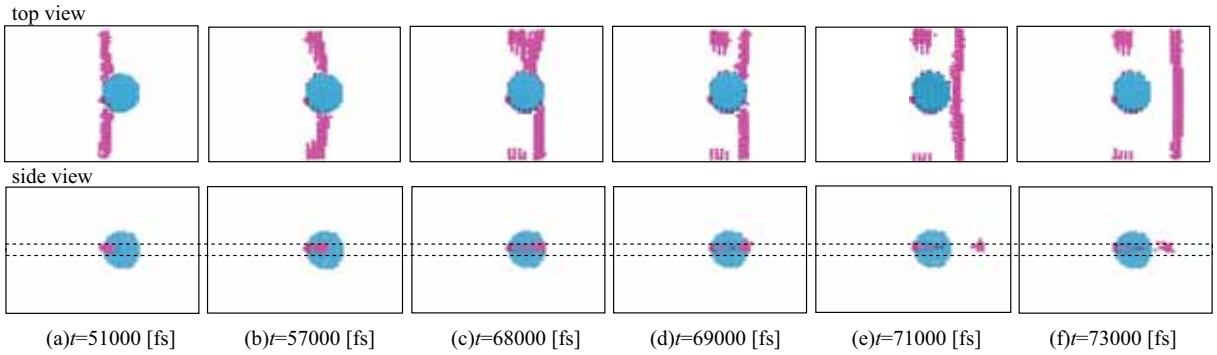

Figure 12: Motion of screw dislocation (L_x=10.4 nm, d = 3.0 nm).

(Fig. 12). Thus, it is difficult to obtain a clear tendency for the interaction between screw dislocation and YO precipitate. In addition, it also should be noted that the present model for screw dislocation has a large difference against the previous edge dislocation; that is, the simulation cell is not periodic in the glide direction and might be too small to mimic the dislocation motion in bulk. In this manner, more sophisticated model is so far needed for screw dislocation, and the present report could be a help for refinement.

5 CONCLUSIONS

We have performed various molecular dynamics simulations on the interaction between edge/screw dislocations and nanosphere of yttria oxide in bcc Iron, targetting the phenomena in oxide dispersion strengthened (ODS) steels. Since there is no all-round interatomic potential functions that can represent all the bonding state, i.e. metal, ion and covalent systems, we have adopted rough approximation that each atom in yttria oxide is not distinguished but treated as "monatomic" pseudo-atom, and its motion is represented with the simple pairwise potential function as same as Johnson potential for Fe. The potential parameters are fitted to the energy change in the hcp infinite crystal, by using the ab-

initio density functional theory (DFT) calculation against explicitly discriminated Y and O. We have observed various dislocation behavior by changing the diameter and periodic distance of the coherently precipitated YO cluster using a periodic slab cell. Although it is also clarified that we might need refinement of the simulation model for screw dislocation, still we have obtained many useful insight on the dislocation/yttria oxide interaction, *e.g.* (1) YO cluster larger than 0.9 nm strongly attracts and traps edge dislocation, (2) highly tensioned screw dislocation easily cut through the precipitate without resistance, and (3) loose screw dislocation shows complicated behavior by changing the slip plane, at the point far away from the precipitate.

REFERENCES

[1] T. Okuda, S. Nomura, S. Shikakura, K. Asabe, S. Tanoue and M. Fujiwara, Proc. Symp. Sponsored by the TMS Powder Metallurgy Committee, Indiana, p.195 (1989)

[2] S. Ukai, T. Nishida, H. Okada, T. Okuda, M. Fujiwara and K. Asabe, Development of Oxide Dispersion Strengthened Ferritic Steels for FBR Core Application, (1) Improvement of Machanical Properties by Recrystallization Processing, Journal of Nuclear Science and Technology, 34 (1997) 256–263.

[3] R. L. Klueh, P. J. Maziasz, I. S. Kim, L. Heatherly, D. T. Hoelzer, N. Hashimoto, E. A. Kenik and K. Miyahara, Tensile and Creep Properties of an Oxide Dispersion-Strengthened Ferritic Steel, Journal of Nuclear Materials, 307–311 (2002) 773–777.

[4] M. Ohnuma, J. Suzuki, S. Ohtsuka, S.-W. Kim, T. Kaito, M. Inoue and H. Kitazawa, A New Method for the Quantitative Analysis of the Scale and Composition of Nanosized Oxide in 9Cr-ODS steel, Acta Materialia, 57 (2009) 5571–5581.

[5] K. Yashiro, M. Naito and Y. Tomita, Molecular Dynamics Simulation of Dislocation Nucleation and Motion at γ/γ' Interface in Ni-Based Superalloy International Journal of Mechanical Sciences, 44 (2002) 1845–1860.

[6] K. Yashiro, F. Kurose, Y. Nakashima, K. Kubo, Y. Tomita and H. M. Zbib, Discrete Dislocation Dynamics Simulation of Cutting of γ' Precipitate and Interfacial Dislocation Network in Ni-Based Superalloys, International Journal of Plasticity, 22 (2006) 713–723.

[7] M. J. Alinger, B. D. Wirth,, H. J. Lee and G. R. Odette, Lattice Monte Carlo Simulations of Nanocluster Formation in Nanostructured Ferritic Alloys, Journal of Nuclear Materials, 367–370 (2007) 153–159.

[8] C. Hin, B. D. Wirth and J. B. Neaton, Formation of Y_2O_3 Nanoclusters in Nanostructured Ferritic Alloys during Isothermal and Anisothermal Heat Treatment: A Kinetic Monte Carlo Study, Physical Review B, 80 (2009) 134118.

[9] G. Kresse and J. Hafner, Ab Initio Molecular Dynamics for Liquid Metals, Physical Review B, 47 (1993) 558–561.

[10] E. N. Maslen, V. A. Streltsov, and N. Ishizawa, Acta Crystallographica B, 52 (1996) 414–422.

[11] D. Vanderbilt, Soft Self-Consistent Pseudopotentials in a Generalized Eigenvalue Formalism, Physical Review B, 41 (1990) 7892–7895.

[12] D. C. Langreth and J. P. Perdew, Theory of Nonuniform Electronic Systems. I. Analysis of the Gradient Approximation and a Generalization that Works, Physical Review B, 21 (1980) 5469–5493.